

# The Influence of Slope Breaks on Lava Flow Surface Disruption

Lori S. Glaze, Goddard Space Flight Center, Greenbelt, MD, USA

Stephen M. Baloga, Proxemy Research, Gaithersburg, MD, USA

Sarah A. Fagents and Robert Wright, HIGP, University of Hawaii, Honolulu, HI, USA

Corresponding author: L. S. Glaze, NASA Goddard Space Flight Center, Code 690, 8800

Greenbelt Road, Greenbelt, MD 20771 (Lori.S.Glaze@nasa.gov)

## Key points

- Basic models are developed for active lava flow surface disruption at a slope break
- Surface disruption can significantly affect core cooling and flow length, depth and advance rate
- Disruption length scales depend on flow regime (laminar vs turbulent) beyond slope break

21 **Abstract** Changes in the underlying slope of a lava flow impart a significant fraction of  
22 rotational energy beyond the slope break. The eddies, circulation and vortices caused by this  
23 rotational energy can disrupt the flow surface, having a significant impact on heat loss and thus  
24 the distance the flow can travel. A basic mechanics model is used to compute the rotational  
25 energy caused by a slope change. The gain in rotational energy is deposited into an eddy of  
26 radius  $R$  whose energy is dissipated as it travels downstream. A model of eddy friction with the  
27 ambient lava is used to compute the time-rate of energy dissipation. The key parameter of the  
28 dissipation rate is shown to be  $\rho R^2/\mu$ , where  $\rho$  is the lava density and  $\mu$  is the viscosity, which  
29 can vary by orders of magnitude for different flows. The potential spatial disruption of the lava  
30 flow surface is investigated by introducing steady-state models for the main flow beyond the  
31 steepening slope break. One model applies to slow-moving flows with both gravity and pressure  
32 as the driving forces. The other model applies to fast-moving, low-viscosity, turbulent flows.  
33 These models provide the flow velocity that establishes the downstream transport distance of  
34 disrupting eddies before they dissipate. The potential influence of slope breaks is discussed in  
35 connection with field studies of lava flows from the 1801 Hualalai and 1823 Keaiwa Kilauea,  
36 Hawaii, and 2004 Etna eruptions.

37

38 **Index terms** 8425 Effusive volcanism  
39 8414 Eruption mechanisms and flow emplacement  
40 8485 Remote sensing of volcanoes

41

42

43

44

## 45 **1. Introduction**

46 When a flow changes direction, the momentum vector of the flow also changes direction.  
47 This results in the production of angular momentum when the flow transits a break in slope or is  
48 directed laterally by confining topography. Under relatively steady eruption conditions, a viscous  
49 lava flow rapidly forms a solid crust that insulates the interior of the flow. If undisturbed, this  
50 crust preserves the mobility of the hot lava core and allows the flow to travel substantial  
51 distances until the lava supply ceases or the interior of the flow cools enough to inhibit further  
52 advance. A comprehensive review of the influence of cooling, crust formation and effusion rate  
53 is contained in *Harris and Rowland* [2009].

54 The angular momentum generated by slope breaks and lateral confinements results in some  
55 form of circulation, eddying or vortex formation within the flow or at its margins. Pulses in lava  
56 supply can also induce circulation in the flow. When such flow patterns disturb the cooler or  
57 crusted surface of the flow, they can have a profound influence on radiative heat loss, viscosity,  
58 incipient crystallization and thus the distance a flow travels [*Finch and Macdonald*, 1953; *Booth*  
59 *and Self*, 1973; *Moore*, 1987; *Rowland and Walker*, 1990; *Crisp and Baloga*, 1990a, b; *Crisp and*  
60 *Baloga*, 1994; *Harris and Rowland*, 2001].

61 The only predictive attempt at calculating the extent of surface disruption appears in *Harris*  
62 *and Rowland* [2001]. It is based on empirical studies of core exposure as a function of flow  
63 velocities in channels and they pointed out that this dependence lacked rigorous quantification  
64 [*Harris and Rowland*, 2001, p.28]. Field measurements and theoretical modeling of the main  
65 flow from the well-documented 1984 Mauna Loa eruption show a marked increase in viscosity 5  
66 km downstream of a major slope break at 10 km along the flow path [*Moore*, 1987; *Harris and*  
67 *Rowland* [2001]. With the slope embedded in the computation of flow velocity, the FLOWGO

68 model of *Harris and Rowland* [2001] predicts such an increase [see Figure 5 in *Harris and*  
69 *Rowland*, 2001] and motivates further study of slope changes and surface disruption.

70 There have now been more than two decades of remote sensing observations of active lava  
71 flows in numerous settings. Such images commonly show relatively broad spikes in spectral  
72 radiance (and derived metrics such as radiant flux) along the flow path that are indicative of  
73 transient or persistent disruptions of the cooler flow surface and a consequent exposure of the  
74 hotter inner core [*James et al.*, 2007; *James et al.*, 2010]. *Wright and Flynn* [2003] and *Wright*  
75 *et al.* [2010] give methods for estimating the core exposure of active flows from high resolution  
76 satellite remote sensing data. Although such data show indications of potential relationships  
77 between slope changes and the disruption of the lava surface, higher spatial resolution remote  
78 sensing data are needed to definitively identify a cause and effect relationship, and to place  
79 observational constraints on the length scales of disruption.

80 The work presented here attempts to predict the extent of flow surface disruption and core  
81 exposure due to a sudden change in the underlying slope. The model is a combination of three  
82 first-order models for different aspects of the problem. A basic mechanics model is used to  
83 approximate the rotational energy caused by a steepening slope change. Similar energy  
84 considerations apply to a shallowing slope change, lateral redirection of the flow by topographic  
85 confinements, channel constrictions and wall effects, breaches, and pulses in the lava supply rate;  
86 the resultant impact of each case on the surface disruption may be different. The gain in  
87 rotational energy is deposited into an eddy whose energy dissipates as it is transported  
88 downstream by the main flow. An elementary model of the friction between the eddy and the  
89 ambient lava provides the rate of energy dissipation as a function of time. The downstream  
90 spatial disruption of the flow surface is subsequently determined with steady-state models for the

91 main flow beyond the slope break: one for slow-moving flows driven by both gravity and  
92 pressure, and another for low-viscosity turbulent flows. Both models of the main flow include a  
93 volume conservation requirement at all points along the path of the flow.

94 The influence of surface disruption on cooling of the lava core is investigated. Implications  
95 in the context of surface disruption are given for field studies of basaltic flows from eruptions at  
96 Mt. Etna, Sicily in 2004, and the Hualalai 1801 and 1823 Kilauea eruptions in Hawaii.

97

## 98 **2. Model Overview**

99 The intent of the model is to develop a first-order estimate for the distance over which the  
100 surface of a steady-state flow is disrupted by a steepening of the underlying slope from one  
101 inclined plane to another. When a surface disruption occurs, it persists for a finite time as it is  
102 transported downstream by the underlying main flow. This duration is referred to here as the  
103 ‘disruption time’. The corresponding ‘disruption length’ is obtained from the disruption time by  
104 knowing the flow velocity. The disruption length is determined by how much rotational energy is  
105 imparted by the slope break and the assumption that this energy goes into vertical circulation  
106 within the flow. This rotational energy then dissipates with time due to friction with the ambient  
107 lava. The model assumes that disruption time is given by the dissipation time.

108 The model considers a vertical column of height  $h$ , width  $w$ , and length  $dx$  along the flow  
109 direction. The width and density of the flow are taken as constants. The column encounters the  
110 break in slope, then rotates to a new orientation at the beginning of the downstream segment  
111 (Figure 1). The pivot of the column is taken as the slope break and no slippage is considered.  
112 For illustration purposes, the slope of the upper reach is taken as zero and the lower reach has  
113 slope  $\phi$  with respect to the horizontal. The assumption is made that the rotational kinetic energy

114 imparted by the slope break is determined by the amount of reorientation of the column to the  
115 normal of the new slope.

116 As a flow moves downslope, there is of course a change in kinetic and potential energy. In  
117 steady state on a constant slope, the kinetic energy of a column remains constant, but the energy  
118 gained from the decrease in potential energy is identically dissipated by the viscous stresses and  
119 is converted to heat. The disruption model presented here investigates the additional rotational  
120 kinetic and potential energies above the steady state main flow values. In absolute terms the  
121 energy changes at the slope break could be very small compared to the downstream steady state  
122 main flow values. However, the transfer of material from the upper layers of the inner core  
123 resulting from the additional rotational energy can have a significant influence on the thermal  
124 balance.

125 The conservation of kinetic, potential and rotational energy is used to find the new boundary  
126 conditions at the beginning of the downstream segment of the flow. The volumetric flow rate is  
127 conserved throughout the upstream and downstream segments of the flow. Two cases are  
128 considered for the nature of the flow on the lower slope. One considers the flow to be essentially  
129 laminar with the possibility that both gravity and pressure are the driving forces. The other uses  
130 a gravity-driven hydraulic model more appropriate to a turbulent lava flow. Various details of the  
131 main flow models appear in the appendices.

132 The induced circulations, eddies, and vortices are modeled approximately as a rotating  
133 cylinder oriented transverse to the main flow direction. Although many types of flow  
134 circulations are possible, they are referred to collectively as ‘eddies’ throughout this work. The  
135 model assumes that the eddies cause a surface disruption that persists essentially as long as do  
136 the eddies. The eddies dissipate within the flow as they are transported downstream. In the

137 model, the eddies generated by the slope break are simply carried by the main flow and draw no  
138 energy from the change in downstream potential energy. The dissipation rate is computed by  
139 estimating the energy lost due to eddy circulation against a viscous ambient fluid. This lost  
140 energy is removed from the eddy as the main flow travels downstream until the energy loss  
141 accumulates to a final value. For a given eddy radius, angular velocity, and viscosity, the  
142 persistence time can thus be calculated and determines the downstream eddy propagation  
143 distance. The variables for the quantitative description of this model are given under Notation.

144

## 145 **2.1 Mechanics at the Slope Break**

146 In going from one slope to the other, the normal to the original upstream surface rotates  
147 through an angle  $\theta(t)$  from 0 at  $t = 0$  to a new position with  $\theta(t_f) = \phi$ . At the completion of the  
148 rotation, the column is aligned with the new normal to the downstream surface (see Figure 1).  
149 The time it takes to complete this rotation is  $t_f$ . At  $t = 0$ , just before rotation begins as the column  
150 encounters the slope break, the column has translational kinetic energy,

151

$$152 \quad KE = \frac{1}{2} mu^2, \quad (1)$$

153

154 where  $m$  is the mass of the column and  $u$  is the flow velocity upstream of the slope break.

155 Across the slope break the column is treated as a physical pendulum of length  $h$  and angular  
156 velocity  $\omega$ . The center of mass of the column drops due to the rotation about the pivot point  
157 adding potential energy to the column in the amount

158

$$159 \quad PE = \frac{1}{2} mgh(1 - \cos\phi), \quad (2)$$

160

161 where  $g$  is the acceleration due to gravity. The sum of the kinetic energy and the change in  
162 potential energy goes into two quantities, rotational kinetic energy and translational kinetic  
163 energy immediately after the slope break.

164 Using the approximation for the moment of inertia of the column,  $I = mh^2/3$ , the angular  
165 acceleration is given by

166

$$167 \quad \frac{d^2\theta}{dt^2} = \frac{3g \sin\theta(t)}{2h}, \quad \text{where } \theta(0) = 0, \quad \omega = \omega(0) = u/h. \quad (3)$$

168

169 The elementary solution where  $\sin\theta \approx \theta$  is

170

$$171 \quad \theta(t) = \sqrt{\frac{u^2}{6gh}} (e^{t/\tau} - e^{-t/\tau}) \leq \phi, \quad \text{where } \tau = \sqrt{\frac{2h}{3g}}. \quad (4)$$

172

173 The initial rotational kinetic energy,  $KE_{rot}$ , at the slope break is given by

174

$$175 \quad \begin{aligned} KE_{rot}(0) &= \frac{1}{2} I \omega(0)^2 = \frac{1}{2} \frac{mh^2}{3} \left(\frac{u}{h}\right)^2 \\ &= \frac{1}{6} mu^2, \quad \text{for } h > 0. \end{aligned} \quad (5)$$

176

177 Equation (5) shows that as the column begins to pivot over the slope break, the rotational  
178 energy is one-third that of the incident translational kinetic energy given by equation (1). At the



179 completion of the rotation about the pivot point, at  $t = t_f$ , the rotational kinetic energy imparted  
 180 by the slope break is

181

$$\begin{aligned}
 182 \quad KE_{rot}(t_f) &= \frac{1}{2} I \omega(t_f)^2 = \frac{1}{2} \frac{mh^2}{3} \left( \frac{u}{2h} \right)^2 \left( e^{t_f/\tau} + e^{-t_f/\tau} \right)^2 \\
 &= \frac{1}{24} mu^2 \left( e^{t_f/\tau} + e^{-t_f/\tau} \right)^2, \quad \text{for } h > 0.
 \end{aligned}
 \tag{6}$$

183

184 Across the slope break an energy balance can thus be constructed. The incoming kinetic  
 185 energy from equation (1), plus the change in rotational kinetic energy from equations (5) and (6),  
 186 plus the gain in potential energy from equation (2), must go into the outgoing kinetic energy of  
 187 the column,

188

$$189 \quad \frac{mu^2}{2} + \frac{I\omega(0)^2}{2} + \frac{mgh}{2} (1 - \cos\phi) - \frac{I\omega_f^2}{2} = \frac{mu_2^2}{2}, \tag{7}$$

190

191 where  $\omega_f$  is the angular velocity of the column after it has rotated through  $\phi$  to its new  
 192 orientation. Equation (7) with flow rate conservation ( $uh = u_2h_2$ ) can be solved to obtain the  
 193 outgoing velocity,  $u_2$ , on the immediate downstream side of the slope break with the selection of  
 194 the physically appropriate roots. The same type of energy balance applies when a slope shallows.  
 195 The main difference would be the subsequent boundary conditions and the nature of the  
 196 governing transport equation beyond the slope break. A more refined approach would  
 197 investigate a continuous deformation of the column across the slope break, but that requires  
 198 solution of the Navier-Stokes equation and is beyond the scope of the present work.

199 The exit value of the velocity  $u_2$  changes very little ( $<0.5\%$ ) from the incident conditions for  
200 slopes ( $<15^\circ$ ) relevant to most lava flows. This is because the energy balance in equation (7)  
201 predominantly puts the gains in potential energy into the rotational energy that increases with  
202 slope, leaving the exit flow conditions essentially unchanged. For practical purposes, therefore,  
203 these velocity changes can be ignored.

204 The absolute value of the rotational energy per kg changes substantially with the slope and  
205 the incident conditions, as shown in Figure 2. The vertical axis gives the exit rotational energy  
206  $KE_{rot}(t_f)$  per kg as a function of the change in underlying slope. The relative changes in the  
207 rotational kinetic energy are illustrated by considering three flow depths ( $h = 1, 3$  and  $6$  m; gray,  
208 red, and green curves, respectively) and two incident flow velocities ( $u = 1$  and  $2$  m  $s^{-1}$ ; solid and  
209 dashed curves, respectively). The rotational energy acquired from the slope break increases with  
210 incident flow thickness and changes by factors of 2, 4, and 7 (gray, red, green curves) for the  
211 thicknesses shown over slope changes up to  $15^\circ$ . When the incident velocity is doubled (dashed  
212 curves), there is the same dependence on flow depth and slope, but there is an additional overall  
213 increase in the rotational energy, as expected. A much greater sensitivity to slope is found by  
214 changing the flow depth keeping the velocity constant.

215

## 216 **2.2 Eddy Dissipation**

217 Eddies are produced by the angular momentum generated by the slope break. In the first-  
218 order model used here, the eddy is treated as a cylinder of fluid with radius  $R$  that rotates as it is  
219 transported downstream by the main flow. The best case for the persistence of an eddy is when  
220 its surface is in contact only with the ambient fluid that transports it. In the worst case, an eddy  
221 contacts counter-rotating neighboring eddies and breaks into smaller ones.

222 At time  $t = t_f$ , the rotation of the lava column due to the slope break is completed and an eddy  
 223 is established. The time of eddy dissipation is then measured with time beginning at  $t_f$ . The  
 224 rotational kinetic energy from the slope break is deposited into rotational energy of the eddy,  
 225 thus

$$226 \quad KE_{rot}(t_f) = \frac{1}{2} I_e \omega_{eo}^2 = \frac{1}{2} \left( \frac{1}{2} m_e R^2 \right) \omega_{eo}^2, \quad (8)$$

227 where  $m_e$  and  $I_e$  are the mass and moment of inertia of the eddy, respectively. The initial angular  
 228 velocity of the eddy rotation,  $\omega_{eo}$ , can be found by re-arranging equation (8) to be

$$229 \quad \omega_{eo} = \sqrt{\frac{4KE_{rot}(t_f)}{R^2 m_e}} = \frac{2}{R} \sqrt{\frac{KE_{rot}(t_f)}{m_e}} = \frac{2}{R} \sqrt{\frac{m}{m_e} \frac{KE_{rot}(t_f)}{m}}, \quad (9)$$

231 where the rotational kinetic energy per unit mass is obtained from the energy balance for the  
 232 column in equation (6).

234 The resistive force on the eddy due to ambient lava is approximated by

$$235 \quad F = \mu A_e \frac{dv}{dr} \approx \mu A_e \omega_e(t), \quad (10)$$

237 where  $A_e$  is the surface area of the eddy in contact with ambient lava. Assuming the eddy retains  
 238 its integrity, cumulative energy lost due to friction over time beginning with  $t_f$  is given by

$$239 \quad W_{diss}(t) = \int_{t_f}^t F ds \approx \mu A_e \int_{t_f}^t \omega_e(t) ds = \mu (2\pi R w) \int_{t_f}^t \omega_e(t) \frac{ds}{dt} dt, \quad t \geq t_f. \quad (11)$$

242

243 The variable  $s$  is the distance a point on the cylinder travels to dissipate the energy  $W_{diss}$  by  
244 friction with the ambient fluid, given by

245

$$246 \quad s(t) = R \int_{t_f}^t \omega_e(t) dt = R \omega_{e0} \frac{\Gamma}{4} \left( 1 - e^{-4(t-t_f)/\Gamma} \right). \quad (12)$$

247

248 To determine the amount of dissipation after the onset of eddy rotation,  $\omega_e(t)$  must also be  
249 determined. The time dependence for the deceleration of eddy rotation due to friction is found  
250 from Newton's 2<sup>nd</sup> law

251

$$252 \quad I_e \frac{d\omega_e}{dt} = -FR \approx -\mu A_e \omega_e R. \quad (13)$$

253

254 Integrating equation (13), we obtain

255

$$256 \quad \int_{\omega_{e0}}^{\omega_e(t)} \frac{d\omega_e}{\omega_e} = -\frac{2\mu A_e}{m_e R} \int_{t_f}^t dt, \quad (14)$$

257

258 and an expression for  $\omega_e(t)$  is found to be,

259

$$260 \quad \omega_e(t) = \omega_{e0} e^{-4(t-t_f)/\Gamma}; \quad \text{where } \Gamma = \frac{\rho R^2}{\mu}. \quad (15)$$

261

262 This shows that the critical parameter for eddy dissipation is the time constant  $\Gamma$ . It can also  
 263 be expressed in terms of the Reynolds number of the flow itself,  $Re = \rho u_2 h_2 / \mu$  as  $\Gamma = Re R^2 / q_0$ .  
 264 Fast-moving, high-Re flows will have long time constants and the effects of slope breaks will  
 265 tend to propagate greater distances downstream and vice versa.

266 The rotational energy lost to friction is given by equation (11), using equations (12) and (15),  
 267 as

$$269 \quad W_{diss}(t) = \frac{m_e R^2}{4} \omega_{eo}^2 \left(1 - e^{-8(t-t_f)/\Gamma}\right) = KE_{rot}(t_f) \left(1 - e^{-8(t-t_f)/\Gamma}\right), \quad (16)$$

270  
 271 which yields the time decay of rotational energy due to the friction of the eddy. Curves relevant  
 272 to lava flows are shown in Figure 3. Slightly more than half (55%) the initial rotational energy is  
 273 dissipated by friction in 0.1 time constant, 98% is dissipated in half a time constant, and 99.99%  
 274 is dissipated when  $t-t_f = \Gamma$ . Thus  $\Gamma$  is a reasonable estimate of the dissipation time and, by  
 275 assumption, the disruption time.

### 277 **2.3.1 Eddy Size**

278 Many factors could influence the circulation of a flow as it traverses a change in slope or  
 279 encounters a topographic barrier. These include the character of the incident flow (laminar,  
 280 turbulent, or disrupted), roughness of the flow bed, the presence of entrained and incipient solids,  
 281 and interactions with channel walls. All such factors require independent theoretical or empirical  
 282 studies.

283 There is a link between the volume of the fluid column and the volume of the eddy that is the  
 284 recipient of the rotational energy imparted by the slope break. To embrace a range of eddy sizes,

285 the extent of the column along the direction of flow ( $dx$ ) is prescribed to be the diameter of the  
286 eddy ( $2R$ ; Figure 1). Thus the fraction of column volume that receives the rotational energy is  
287 given by

$$289 \quad \mathfrak{S} = \frac{\text{vol. eddy}}{\text{vol. col.}} = \frac{\pi}{2} \left( \frac{R}{h} \right)^2. \quad (17)$$

290  
291 For a large circulation,  $R$  might approach  $h/2$  as suggested by engineering experience with  
292 turbulent flow in pipes. It is difficult to estimate a minimum relevant size of an eddy in a lava  
293 flow. However, from a practical standpoint a lower limit can be estimated by considering an  
294 incident laminar flow. Appendix A gives the cumulative rotational energy for an incident laminar  
295 flow as it traverses the slope break. Due to the strong dependence of rotational energy on the  
296 height within the flow, only 3% of the rotational energy would come from the lower half of the  
297 flow and only about 11% from the lower two-thirds. The upper 5% of the flow contributes  
298 almost a quarter of the rotational energy and so  $R = 0.1h$  is taken as a practical minimum value  
299 for eddy radius.

300 The time constants for eddy dissipation shown in Table 1 are clearly dominated by the  
301 viscosity and the eddy size, which must be roughly proportional to the flow depth. Figure 3  
302 shows the relative dissipation as a function of time for  $\Gamma = 100, 200, 500$  and  $1000$  s from  
303 equation (16). Low-viscosity lavas imply large time constants, and such flows are predicted to  
304 maintain circulations for long times, tens of seconds or more. Eddies would be carried substantial  
305 distances downstream by any fast-moving segment of the flow. If the flow is turbulent, however,  
306 the simplistic model used here would require significant modification to account for the decay of

307 larger eddies into smaller ones. Conversely, high-viscosity flows could manifest the influence of  
308 circulation by local cooling, stagnation, and inflation.

309 The dominant role of viscosity in determining the extent of surface disruption calls into  
310 question the validity of viscosity estimates derived from field measurement of active flows.  
311 Usually such estimates are derived from the Jeffreys' equation for a steady-state flow of constant  
312 depth [*Nichols*, 1939], although numerous modifications have been made to account for time-  
313 dependent effects [e.g., *Baloga and Pieri*, 1986], lava yield strength [e.g., *Harris and Rowland*,  
314 2001], levee building [e.g., *Glaze et al.*, 2009], and similar factors. These formulations do not  
315 account for the fluid pressure caused by the resulting topographic gradients in the flow. It is  
316 shown in Appendix B that the incorporation of seemingly small pressure gradients causes an  
317 important systematic departure from the steady-state constant depth assumptions of the Jeffreys'  
318 approach. The primary consequence is that evaluations of viscosity based on field measurements  
319 of flow parameters could be overestimated by an order of magnitude or more in the case of thick  
320 (50–200 m) flows on other planetary surfaces.

321

### 322 **3. Implications**

#### 323 **3.1 Influence of Flow Surface Disruption on Core Temperature**

324 The potential influence of surface disruption on the core temperature is illustrated by  
325 considering a schematic flow of constant depth  $h_2$  and velocity  $u_2$  that begins with temperature  $T_o$   
326 at the top of an inclined plane. The core temperature is computed by the basic steady state  
327 radiation loss formula

328

329 
$$T_{core}(x) = T_o \left[ 1 + \frac{3f \varepsilon \sigma T_o^3 h_2 x}{\rho C_p u_2} \right]^{-1/3}, \quad (18)$$

330

331 using the flow parameters given in Table 2, with  $f$  denoting the areal fraction of exposed hot lava  
 332 core within the crusted flow surface, and  $\sigma$  being the Stefan-Boltzmann constant.

333 The degree to which the disrupted upper layer of a lava flow exposes core lava depends upon  
 334 many factors, including the viscosity of the lava and the thickness and mechanical strength of the  
 335 crust. We do not attempt to draw a direct link between the rotational eddies and the ability to  
 336 actually “disrupt” the surface crust. However, several cases exploring a range of potential  $f$   
 337 values can be explored to place bounds on the sensitivity of increased surface disruption over  
 338 short distances.

339 Figure 4 shows the resulting temperature profiles along the length of the flow, for three cases  
 340 having different values of  $f$ . The uppermost curve assumes a core exposure fraction of  $f = 0.05$ ,  
 341 which is somewhat high for most flows [*Crisp and Baloga, 1990a; Oppenheimer, 1991; Wright*  
 342 *et al., 2000; Wright et al., 2010*]. For comparison, the lowermost curve uses an extreme value of  
 343  $f = 0.5$ . The red curve shows the strong influence of the  $T^4$  radiation term when the flow surface  
 344 is disrupted by eddies. Twelve 60 m segments of disruption with  $f = 0.9$  were inserted in the first  
 345 2 km of the flow, followed by three others further downstream. Everywhere else, a value of  $f =$   
 346 0.05 was applied. The disruption in the first 2 km of the flow causes a major drop (35°C) in the  
 347 core temperature. Using equation (3) of *Harris and Rowland [2001]*, such a temperature drop  
 348 would cause the core viscosity to increase by a factor of 4. This would have a significant  
 349 influence on the advance velocity and the depth of the flow. A few segments of surface  
 350 disruption upstream will have a significant impact on the ultimate flow length.



351

### 352 **3.2 The September 2004 Lava Flow at Mt. Etna**

353 A relatively well-documented flow-producing eruption exemplifying laminar flow (Appendix  
354 B) occurred at Mt. Etna, Sicily in 2004-2005 [e.g., *Mazzarini et al.*, 2005; *Burton et al.*, 2005].  
355 Comprehensive dimensional data on the flow were acquired by airborne laser altimetry  
356 *Mazzarini et al.* [2005]. Analysis of 162 profiles indicated a typical flow thickness of 5 m,  
357 although there is considerable variability, with a maximum of 17 m. Both *Mazzarini et al.* [2005]  
358 and *Wright et al.* [2010] show that 20–30° slopes are common, and field observations obtained  
359 from the *Global Volcanism Network* [2004] suggest that 1 m s<sup>-1</sup> is a representative flow velocity.  
360 The eddy dissipation relationship (Figure 3) shows that the influence of slope changes (or  
361 equivalent influences) decays in ~0.5–2 min. for  $\Gamma \sim 100\text{--}200$  s. With channel velocities of 1 m  
362 s<sup>-1</sup>, this corresponds to disruption lengths of 30–120 m. In Appendix B, it is shown that the use of  
363 the Jeffreys' equation (commonly used for flow velocity calculations) can significantly  
364 overestimate the viscosity of active flows, so a dissipation time on the order of hundreds of  
365 seconds may be reasonable. If the lava viscosity was significantly in excess of hundreds of Pa s,  
366 the dissipation time could be on the order of seconds to a few tens of seconds for eddies of  $\leq 1$  m  
367 and a flow thickness of 5 m. However, significant slope changes occur about every 100 m along  
368 the 2004 Mt. Etna flow path. Even with a relatively rapid dissipation rate, the repeated slope  
369 changes at length scales comparable to the dissipation lengths keep adding flow circulation and  
370 surface disruption.

371 One potentially useful approach to validating and placing constraints on the proposed model  
372 is to correlate changes in lava flow surface temperature, derived from remote sensing thermal  
373 imaging, with underlying surface topography and slopes. However, the spatial resolution of even

374 some of the best orbiting thermal imagers, such as Hyperion (30 m pixels), is insufficient. In  
375 order to distinguish changes in surface radiance on the order of the disruption scales (30 – 120 m  
376 for a flow like the 2004 Mt. Etna flow) requires spatial resolutions about an order of magnitude  
377 finer (~5-10 m pixels). One approach for future work is to use field thermal imagers that are  
378 capable of spatial resolutions on the order of 5-10 m/pixel (or better), with specific application to  
379 this problem to ensure synoptic coverage over the full length of possible disruption. Such field  
380 campaigns have successfully documented variations in lava flux [*James et al.*, 2007; *James et*  
381 *al.*, 2010]. In particular, *James et al.* [2007] examine the time dependent thermal flux of several  
382 lava flows during the 2004-2005 eruption at Mt. Etna that progress from a steeper to a shallower  
383 slope. A similar technique would be appropriate here for lava flowing onto a steeper slope. It is  
384 important to note that such a field campaign must adequately characterize the time dependent  
385 changes in thermal flux owing to pulses in lava flux in order to distinguish the systematic surface  
386 disruption due to the change in slope.

387

### 388 **3.3 The 1801 Hualalai Flow, Hawaii**

389 The possibility of turbulent lava flows has been postulated for many years [e.g., *Nichols*,  
390 1939, p.294; *Shaw and Swanson*, 1970; *McGetchin and Eichelberger*, 1975; *Baloga et al.*, 1995].  
391 Turbulence can be caused not only by high flow velocities and low viscosities, but also  
392 constrictions and widenings of the flow, small and large-scale topographic variations, and the  
393 motions of entrained crystals and ambient materials. Although there is some disagreement on the  
394 eruption rates during the 1801 Hualalai lava flow [*Kaauhikaua et al.*, 2002], with viscosity  
395 determined by petrologic studies to lie in the range  $10^1$ – $10^2$  Pa s, and field estimates of flow  
396 velocities of  $\sim 10$  m s<sup>-1</sup>, the 1801 Hualalai eruption likely produced at least transient turbulent

397 lava flows with depths of ~5 m near the source. The uncommonly deep (6–18 m) downstream  
398 channels may have formed in part through construction due to very short duration overflow  
399 events, however, even partially full, greater turbulence through these stretches is expected  
400 [McGetchin and Eichelberger, 1975; Guest et al., 1995].

401 The 1801 Hualalai flow also traversed several large changes in slope (3–6°) along the flow  
402 path [Baloga et al., 1995]. Xenoliths were deposited as bedload at the beginning of the final  
403 reach toward the ocean. From that point, the decay of these circulations and intense cooling  
404 produced a morphology common to other basaltic channelized flows on low slopes.

405 The elementary turbulent flow model in Appendix B indicates that such a flow would reach  
406 the terminal velocity on a flat plane in tens to ~100 m from the source or slope break. Using the  
407 range of likely terminal velocities (5–15 m s<sup>-1</sup>) suggested in Baloga et al. [1995], the computed  
408 disruption lengths are shown in Figure 5 for appropriate Hualalai parameters ( $\rho = 2600 \text{ kg m}^{-3}$ ,  $h$   
409 = 5 m,  $R_1 = 1 \text{ m}$ ,  $\phi = 10^\circ$ ) and viscosities of 50–500 Pa s spanning the range identified by  
410 McGetchin and Eichelberger [1975]. With the eddy radius taken as only 20% of the flow depth,  
411 the computed flow disruptions extend for hundreds of meters to a kilometer or so. The  
412 circulations gained from the slope breaks most likely contributed significantly to the suspension  
413 of the xenoliths. Given that there are several slope breaks along the flow, such disruption lengths  
414 are consistent with the complex morphologic features of the flow [McGetchin and Eichelberger,  
415 1975; Baloga et al., 1995; Guest et al., 1995] until the very shallow slopes near the ocean.

416

### 417 **3.4 The 1823 Keaiwa “Great Crack” Flow, Kilauea Volcano, Hawaii**

418 The 1823 Keaiwa flow from the Great Crack fissure at Kilauea also produced rapidly moving  
419 low-viscosity flows. Near the source Guest et al. [1995] estimated the velocity at 15 m s<sup>-1</sup>. Field

420 evidence suggests a source depth of  $<0.5$  m with a downstream thickening in distal regions to  
421 only 1–2 m near the ocean [*Guest et al.*, 1995; *Baloga et al.*, 1995; and sources cited therein].  
422 The predominant underlying slope is about  $5^\circ$  from the fissure to the ocean (a distance of  $\sim 4$  km  
423 using Area 2 of Figure 4 from *Baloga et al.* [1995]). The flow apparently issued from the Great  
424 Crack as a rapidly moving sheet, transitioning to a slabby ‘a’a at the distal margins. The  
425 turbulent main flow model (Appendix B), using the parameters  $u(0) = 15 \text{ m s}^{-1}$ ,  $h(0) = 0.5 \text{ m}$ ,  $\phi_2$   
426  $= 5^\circ$  and  $h_2^* = 2 \text{ m}$ , indicates that the flow would attain a velocity  $u_2$  of  $3.75 \text{ m s}^{-1}$  in  $\sim 100 \text{ m}$ .  
427 Thus, the 4 km transit time to the ocean would be  $\sim 1000 \text{ s}$ . The model used in *Baloga et al.*  
428 [1995] assumed a constant velocity of  $10 \text{ m s}^{-1}$  from the fissure to the ocean resulting in a transit  
429 time about half this value. With a velocity of  $3.75 \text{ m s}^{-1}$ ,  $R \approx 0.5\text{--}1 \text{ m}$  and  $\mu = 100 \text{ Pa s}$ , Table 1  
430 suggests a disruption length of about 24–98 m. Due to the thinness of the flow, small-scale  
431 topographic variations could occur over such a disruption length, feeding the slope induced  
432 circulations. The resulting mixing would have contributed to the homogeneity of the advancing  
433 sheet, but the transit time was evidently too short to permit a significant increase in the viscosity.

434

#### 435 **4. Summary and Conclusions**

436 Changes in slope or the lateral redirection of a lava flow impart a significant fraction of the  
437 incident kinetic energy of the flow into rotational energy. For steepening slopes, the eddies,  
438 circulation and vortices caused by this rotational energy can disrupt the flow surface and have a  
439 significant impact on the heat loss and thus the distance the flow can travel. The quantity of  
440 rotational energy imparted to the downstream flow is more sensitive to the flow depth than the  
441 incident flow velocity. There is a relatively large quantity of potential energy available from the  
442 main flow compared to the rotational energy of eddies that disrupt the surface and alter the

443 thermal balance. The preliminary model presented in this work does not draw energy from the  
444 main flow. Repeated slope changes and rough topography could significantly extend the  
445 disruption of the flow surface. Many lava flows experience multiple slope breaks of various  
446 magnitudes that can combine to disrupt the surface. A more refined theoretical treatment and  
447 comprehensive field measurements are needed to explore this possibility.

448 This work provides only a first-order analysis of the essential steps in disrupting a lava flow  
449 surface to the extent that it could affect the thermal heat balance of the flow. Consequently, there  
450 are numerous opportunities for improvement at each step of the analysis. First, in transitioning an  
451 abrupt slope break, a continuum approach based on Navier-Stokes equations would provide a  
452 refinement. Relaxing the assumption of an abrupt slope change is also a more realistic approach.

453 The physics of eddy dissipation is another area for future study. Circulations, particularly if  
454 turbulence is generated, are three-dimensional, unlike the planar assumptions used here. This  
455 suggests that a horizontal component of rotation and dissipation must also be included. Lateral  
456 confinements, wall effects, and changes in the lateral direction of the flow path could contribute  
457 significantly to the rotational energy of the flow and thus to surface disruption. Unlike the simple  
458 estimate used here, the physical sizes of the eddies diminishes as they propagate downstream.  
459 The details of how these considerations affect the heat balance are reserved for a future study.  
460 Nonetheless, such improvements in the theory might provide a basis for future field studies and  
461 approaches to flow and eruption dynamics inferred by remote sensing.

462 Besides the parameters of the incident flow, this work shows that the primary factors  
463 controlling the surface disruption are the size of the eddies and the viscosity of the downstream  
464 ambient lava. The model results obtained in this work are at least qualitatively consistent with  
465 surface disruptions interpreted for the fast-moving flows from the 1801 Hualalai and 1823

466 Keaiwa eruptions, as well as a recent flow at Mt. Etna. Future avenues for developing model  
 467 constraints include comparison of predicted disruption lengths with high spatial resolution  
 468 thermal remote sensing data. Future modeling work will include investigation of other likely  
 469 contributors to circulations and surface disruption in active lava flows.

470

## 471 **Appendix A: Cumulative Rotational Kinetic Energy**

472 Here the cumulative rotational kinetic energy of the column in laminar flow as it encounters an  
 473 abrupt slope break is calculated. Within the flow, the velocity profile is taken as

474

$$475 \quad u(z) = \frac{\rho g \sin \theta_1}{\mu} z \left( h_1 - \frac{z}{2} \right), \quad (\text{A1})$$

476

477 where  $h_1$  is an arbitrary height within the flow interior up to the top surface at  $h$ . The upstream  
 478 surface is assumed to be inclined to the horizontal at an angle  $\theta_1$ . If there is no inclination of the  
 479 upper surface, the flow is driven by a constant pressure (momentum flux) and the calculation  
 480 proceeds replacing  $g \sin \theta_1$  with  $gdh/dx$

481 The rotational kinetic energy up to  $h_1$  is

482

$$483 \quad KE_{rot}(h_1) = \frac{I(h_1)\omega(h_1)^2}{2} = \frac{1}{2} \frac{\rho h_1^3 w dx}{3} \left( \frac{u(h_1)}{h_1} \right)^2, \quad (\text{A2})$$

$$= \frac{1}{2} \frac{\rho h_1^3 w dx}{3} \left( \frac{g \sin \theta_1 h_1^2}{2\nu h_1} \right)^2 = \frac{1}{24} \frac{\rho g^2 (\sin \theta_1)^2 h_1^5 w dx}{\nu^2}$$

484

485 where,  $\nu$  is the lava kinematic viscosity ( $= \mu/\rho$ ). Note that the moment of inertia and the angular  
486 velocity depend on  $h_1$  and the strong dependence on the flow depth. Up to the full height  $h$  of the  
487 flow we have:

$$489 \quad KE_{rot}(h_h) = \frac{1}{24} \frac{\rho g^2 (\sin \theta_1)^2 h^5 w dx}{\nu^2} . \quad (A3)$$

490  
491 Thus the cumulative rotational KE fraction as a function of  $h_1$  is

$$493 \quad r = \frac{KE(h_1)}{KE(h)} = \left( \frac{h_1}{h} \right)^5 . \quad (A4)$$

494  
495 This shows, as expected, that the very upper layers of a laminar flow contribute the vast  
496 majority of rotational kinetic energy as the flow goes over an abrupt slope break (see Figure A1).

## 497 498 **Appendix B: Main Flow Transport**

499 The main flow modeling referred to in the text is presented below. The analysis of the  
500 mechanics of the slope break provides the boundary conditions for main flow transport of the  
501 eddies beyond the slope break. The depth and velocity of the main flow may change as a  
502 function of distance beyond the slope break, but the volumetric flow rate is conserved at all  
503 locations downstream.

### 504 505 **The laminar case**

506 The governing equation for the flow depth is taken as

507

$$508 \quad \frac{\partial h_2}{\partial t} + \frac{g \sin \phi h_2^2}{\nu} \frac{\partial h_2}{\partial x} = \frac{g \cos \phi}{3\nu} \frac{\partial}{\partial x} \left( h_2^3 \frac{\partial h_2}{\partial x} \right), \quad (\text{B1})$$

509

510 where  $\nu$  is the kinematic viscosity of the lava ( $= \mu/\rho$ ). The second term on the left-hand side

511 represents gravity as a driving force while the right-hand side represents the influence of fluid

512 pressure. The pressure term is often ignored in volcanologic applications, but is a critical term in

513 hydraulic formulations. Here we consider the steady-state solution of equation (B1). The first

514 integration gives

515

$$516 \quad q_o = u_2(0)h_2(0) = \left( \frac{g \sin \phi h_2^3}{3\nu} - \frac{g \cos \phi}{3\nu} h_2^3 \frac{dh_2}{dx} \right) = u_2(x)h_2(x), \quad (\text{B2})$$

517

518 where  $q_o$  is the volumetric flow rate per unit flow width. A more convenient form is given by,

519

$$520 \quad 1 = \left( \frac{h_2}{h_J} \right)^3 \left( 1 - \cot \phi_2 \frac{dh_2}{dx} \right) \quad (\text{B3})$$
$$h_J = \sqrt[3]{\frac{3q_o\nu}{g \sin \phi_2}}$$

521

522 where  $h_J$  is the oft-cited Jeffreys' steady-state flow depth.

523 Three types of possible behaviors are evident from equation (B3), depending on the boundary

524 conditions ( $u_2(0)$ ,  $h_2(0)$ ), the slope, and the viscosity. The different modes of flow behavior are



525 associated with three roots of equation (B2) or (B3). The critical value that determines the  
526 behavior of the flow is the Jeffreys' flow depth  $h_J$ .

527 What is remarkable about the inclusion of pressure in the steady state is that the Jeffreys'  
528 steady-state flow depth can only be attained for one fortuitous set of conditions of flow rate,  
529 slope, and viscosity and boundary conditions ( $u_2(0)$ ,  $h_2(0)$ ). For  $h_2 < h_J$  ( $u_2 > u_J$ ), the flow must  
530 thin and accelerate as it moves from  $x = 0$ . In steady state, the flow regime actually moves  
531 further away from Jeffreys' conditions with distance from the source until the steady-state  
532 assumption is no longer valid, the viscosity increases due to cooling, or a traveling wave is  
533 established [Mei, 1966].

534 For  $h_2 > h_J$ , the flow must thicken and slow. In this case, the pressure term will always  
535 attempt to drive the flow toward a pond-like topography with  $dh_2/dx \approx \sin\phi_2$ . This has nothing to  
536 do with whether there is a slope break upstream, it is solely a function of the driving forces. The  
537 regimes associated with equation (B3) are clearly analogous to supercritical and subcritical  
538 hydraulics concepts. The tendency to produce an almost horizontal upper surface topography on  
539 shallow slopes may be one of the principal factors causing pahoehoe lobe inflation [Hon *et al.*,  
540 1994; Keszthelyi *et al.*, 1999; Glaze and Baloga, 2013].

541 The analytic solution of equation (B3) is found by changing variables and the boundary  
542 condition

543

$$\psi(\xi(x)) = h_2(x) / h_J, \quad \xi(x) = \tan \phi_2 x / h_J \quad (B4)$$

544

$$\psi(0) = h_2(0) / h_J, \quad \xi(0) = 0$$

545

546 With these changes, the solution of equation (B3) requires integration of

547

$$548 \quad \int \frac{\psi^3 d\psi}{\psi^3 - 1} = \xi . \quad (\text{B5})$$

549

550 The key to the integration of equation (B5) is the expansion of the denominator in terms of the  
551 real and two conjugate roots and the subsequent use of partial fraction expansions.

552

$$553 \quad \int \frac{\psi^3 d\psi}{\psi^3 - 1} = \int \left[ (\psi - 1) \left( \psi + \frac{1}{2} + \frac{i\sqrt{3}}{2} \right) \left( \psi + \frac{1}{2} - \frac{i\sqrt{3}}{2} \right) \right]^{-1} \psi^3 d\psi , \quad (\text{B6})$$

554

555 where  $i = \sqrt{-1}$ . With the use of the partial fraction expansions and considerable algebra, we find

556

$$557 \quad \int \frac{\psi^3 dz}{\psi^3 - 1} = \psi + \ln(\psi - 1)^{1/3} + \frac{\sqrt{3}}{3} \tan^{-1} \left( \frac{\sqrt{3}}{1 + 2\psi} \right) - \ln(\psi^2 + \psi + 1)^{1/6} . \quad (\text{B7})$$

558

559 Thus the solution of equation (B3) in the  $\psi$  variable is

560

$$561 \quad \xi = \psi - \psi(0) + \ln \left( \frac{\psi - 1}{\psi(0) - 1} \right)^{1/3} + \frac{\sqrt{3}}{3} \tan^{-1} \left( \frac{\sqrt{3}}{1 + 2\psi} \right) - \frac{\sqrt{3}}{3} \tan^{-1} \left( \frac{\sqrt{3}}{1 + 2\psi(0)} \right) - \ln \left( \frac{\psi^2 + \psi + 1}{\psi(0)^2 + \psi(0) + 1} \right)^{1/6}$$

562

563 The analytic solution is found by undoing the change of variables from  $\psi$  back to  $h$  using  
564 equation (B4). The analytic solution then gives the longitudinal flow profile  $h(x)$ . Because the  
565 flow rate is constant along the flow path, equation (B2) then provides  $u(x)$ .

566 Figure B1 illustrates the dramatic influence of pressure on the longitudinal thickness profiles  
567 compared to a constant Jeffreys solution, for a flow rate and viscosity and slope that give  $h_J = 5$   
568 m. For clarity of illustration, the slope is taken as  $0.2^\circ$ . Once the flow rate, slope and viscosity  
569 are fixed, small increases in the flow depth at the source cause a significant departure from the  
570 constant Jeffreys' flow depth. The most important consequence of this analysis is that field  
571 estimates using Jeffreys' equation can significantly overestimate the viscosity. Figure B1 shows  
572 that at 3–4 km from the source, the flow has more than doubled beyond  $h_J$ . Because viscosity  
573 estimates go as  $h^3$ , the viscosity estimate would be overestimated by at least an order of  
574 magnitude. This sensitivity suggests that field measurements should measure the topographic  
575 gradient as well as the flow depth as is commonly done in hydrologic applications.

576

### 577 **The turbulent case**

578 Under conditions of turbulent flow, following the formalism of basic hydraulics, the re-  
579 oriented column on the lower reach (see Figure 1) experiences only two forces, gravity and flow  
580 bed resistance characterized by a single parameter, the bed stress. Consistent with a first-order  
581 analysis, the governing equation is taken as

582

$$583 \quad m \frac{du_2}{dt} = mg \sin \phi - \sigma_b A, \quad (\text{B8})$$

584

585 where  $\sigma_b$  is the stress at the flow bed and  $A$  is the area of bed contact with the flow.

586 The common hydraulic application of this formulation is to empirically relate the bed stress  
587 under many different types of ambient conditions (e.g., bed roughness, channel geometry) to an

588 equilibrium flow depth. Similarly, a prescribed value of  $h_2^*$  is used here. With such an  
 589 assumption, and the conservation of flow rate, equation (B8) reduces to

590

$$591 \quad u_2 \frac{du_2}{dx} = g \sin \phi \left( 1 - \frac{h_2^*}{h_2} \right) = g \sin \phi \left( 1 - \frac{h_2^* u_2}{q_o} \right), \quad \text{with } q_o = h_2(0) u_2(0). \quad (\text{B9})$$

592

593 The velocity is given by

594

$$595 \quad u(0) - u_2 - \frac{1}{\alpha} \ln \left( \frac{1 - \alpha u_2}{1 - \alpha u(0)} \right) = \alpha g \sin \phi x, \quad \text{with } \alpha = h_2^* / q_o. \quad (\text{B10})$$

596

597 This solution in general also has two regimes of flow behavior, but they approach the  
 598 equilibrium flow depth  $h_2^*$  from above and below this depth. As the flow depth changes with  
 599 distance, there are corresponding changes in the flow velocity to keep the flow rate constant. The  
 600 simple model above assumes the flow is planar (i.e., infinitely wide), unlike actual flows with  
 601 lateral confinement. Recent advances in hydraulic engineering show how to extend this  
 602 elementary formulation to account for secondary flows within the main flow and the influence of  
 603 narrow and wide stress-inducing lateral boundaries [*Guo and Julien, 2005*].

604

## 605 Notation

|     |       |  |
|-----|-------|--|
| 606 | $A$   | area of contact between turbulent flow and flow bed (constant), $\text{m}^2$ |
| 607 | $A_e$ | area of contact between eddy and ambient lava (constant), $\text{m}^2$       |
| 608 | $C_p$ | specific heat capacity of lava, $\text{J kg}^{-1} \text{K}^{-1}$             |
| 609 | $dx$  | length of column in direction of incident flow (variable), m                 |

|     |               |   |
|-----|---------------|---|
| 610 | $f$           | fraction of exposed lava core   |
| 611 | $F$           | resistive force acting on eddy, N   |
| 612 | $g$           | acceleration due to gravity, $\text{m s}^{-2}$  |
| 613 | $h$           | depth of the incident flow (constant), height of column entering slope break, m                       |
| 614 | $h_2^*$       | equilibrium turbulent flow depth on lower surface (constant), m                                       |
| 615 | $h_2$         | flow depth on lower (2 <sup>nd</sup> ) surface (space dependent), m                                   |
| 616 | $h_2(0)$      | flow depth on lower (2 <sup>nd</sup> ) surface after column rotation (constant), m                    |
| 617 | $h_J$         | Jeffreys' steady-state flow depth, m  |
| 618 | $I$           | moment of inertia of column (constant), $\text{kg m}^2$   |
| 619 | $I_e$         | moment of inertia of eddy (constant), $\text{kg m}^2$   |
| 620 | $KE$          | translational kinetic energy of the incident flow (constant), J                                       |
| 621 | $KE_{rot}(0)$ | initial rotational kinetic energy of the incident flow (constant), J                                  |
| 622 | $m$           | mass of the column (constant), kg   |
| 623 | $m_e$         | mass of eddy (constant), kg   |
| 624 | $PE$          | potential energy gained by column rotation (variable), J  |
| 625 | $q_o$         | lava volume flow rate per unit channel width, $\text{m}^2 \text{s}^{-1}$                              |
| 626 | $r$           | cumulative rotational kinetic energy fraction for laminar flow  |
| 627 | $R$           | radius of circulating eddy (constant), m  |
| 628 | $s$           | distance on the eddy through which the resistive force $F$ acts (time dependent), m                   |
| 629 | $t$           | time, s   |
| 630 | $t_f$         | time required to rotate column through an angle $\phi$ (variable), s                                  |
| 631 | $T_o$         | initial lava core temperature (K)   |
| 632 | $T_{core}$    | temperature of lava core (K)  |
| 633 | $u$           | velocity of the incident flow (constant), $\text{m s}^{-1}$   |
| 634 | $u_2$         | flow velocity on lower (2 <sup>nd</sup> ) surface (space dependent), $\text{m s}^{-1}$                |
| 635 | $u_2(0)$      | flow velocity on lower (2 <sup>nd</sup> ) surface after column rotation (constant), $\text{m s}^{-1}$ |
| 636 | $w$           | width of flow (constant), m   |

|     |                |  |
|-----|----------------|--|
| 637 | $W_{diss}$     | energy lost from eddy due to friction with ambient lava (time dependent)                 |
| 638 | $\Gamma$       | time constant for eddy dissipation (constant), s   |
| 639 | $\varepsilon$  | lava emissivity  |
| 640 | $\theta$       | angle through which column rotates (time dependent)                                      |
| 641 | $\mu$          | dynamic viscosity of lava (constant), Pa s   |
| 642 | $\nu$          | kinematic, viscosity of lava (constant), $\text{m}^2 \text{s}^{-1}$                      |
| 643 | $\rho$         | lava density   |
| 644 | $\sigma$       | Stefan-Boltzmann constant, $5.670373(21) \times 10^{-8} \text{ W m}^{-2} \text{ K}^{-4}$ |
| 645 | $C_p$          | specific heat of lava  |
| 646 | $T$            | lava core temperature  |
| 647 | $\sigma_b$     | bed stress for resistance to turbulent flow (constant)                                   |
| 648 | $\tau$         | time constant for angular rotation of column (constant), s                               |
| 649 | $\phi$         | slope of the flow bed after the slope break (constant)                                   |
| 650 | $\omega$       | angular velocity of column (time-dependent)  |
| 651 | $\omega_e$     | angular velocity of eddy rotation (time-dependent)                                       |
| 652 | $\omega_{eo}$  | initial angular velocity of eddy rotation (constant)                                     |
| 653 | $\omega_f$     | angular velocity of column after it has rotated through angle $\phi$ (constant)          |
| 654 | $\mathfrak{S}$ | ratio of eddy volume to column volume  |

655

656       **Acknowledgments.** Work performed by SMB and LSG was sponsored by NASA grants  
657 NNX10AP63G and NNXAR10G. LSG also acknowledges partial support from the NASA  
658 Planetary Geology and Geophysics program (WBS 811073.02.01.05.80).

659

## 660 **References**

- 661 Baloga, S., and D. Pieri (1986), Time dependent profiles of lava flows, *J. Geophys. Res.*, *91*,  
662 9543–9552.
- 663 Baloga, S. M., P. D. Spudis, and J. E. Guest (1995), The dynamics of rapidly emplaced terrestrial  
664 lava flows and implications for planetary lava flows, *J. Geophys. Res.*, *100*, 24,509–24,519.

- 665 Booth, B., and S. Self (1973), Rheological features of the 1971 Mt Etna lavas, *Proc. Roy. Soc.*  
666 *Lond., Ser. A*, 274, 99–106.
- 667 Burton, M. R., et al. (2005), Etna 2004-2005: An archetype for geodynamically-controlled  
668 effusive eruptions, *Geophys. Res. Lett.*, 32, L09303 doi:10.1029/2005GL022527.
- 669 Crisp, J. A., and S. M. Baloga (1990a), A model for lava flows with two thermal components, *J.*  
670 *Geophys. Res.*, 95, 1255–1270.
- 671 Crisp, J. A., and S. M. Baloga (1990b), Methods for estimating eruption rates of planetary lava  
672 flows, *Icarus*, 85, 512–515.
- 673 Crisp, J. A., and S. M. Baloga (1994), Influence of crystallization and entrainment of cooler  
674 material on the emplacement of basaltic aa lava flows, *J. Geophys. Res.*, 99, 11,819–11,831.
- 675 Finch, R. H., and G. A. Macdonald (1953) Hawaiian volcanoes during 1950, *U.S. Geol. Surv.*  
676 *Bull.*, 996-B, 89pp.
- 677 Glaze, L., S. M. Baloga, W.B . Garry, S. A. Fagents, and C. Parcheta (2009), A hybrid model for  
678 leveed lava flows: Implications for eruption styles on Mars, *J Geophys Res*, 114, E07001, doi:  
679 10.1029/2008je003278.
- 680 Glaze, L. S., and S. M. Baloga (2013), Simulation of inflated pahoehoe lava flows, *J. Volcanol.*  
681 *Geotherm. Res.*, 255, 108–123
- 682 Global Volcanism Network (2004), Mt. Etna, *Bull. Global Volc. Network*, 29(4), Smithson. Inst.,  
683 Wash. D.C.
- 684 Guest J., P. Spudis, R. Greeley, G. J. Taylor, and S. M. Baloga (1995), Emplacement of xenolith  
685 nodules in the Kaupulehu lava flow, Hualalai volcano, Hawaii, *Bull. Volcanol.*, 57, 117–126.
- 686 Guo, J., and P. Y. Julien (2005), Shear stress in smooth rectangular open-channel flows, *J.*  
687 *Hydraul. Eng.*, 131, 30–37.
- 688 Harris, A. J. L., and S. K. Rowland (2001), FLOWGO: a kinematic thermo-rheological model for  
689 lava flowing in a channel, *Bull. Volcanol.*, 63, 20–44.
- 690 Harris, A. J. L., and S. K. Rowland (2009), Effusion rate controls on lava flow length and the  
691 role of heat loss: a review, in *Studies in Volcanology: The Legacy of George Walker*, edited by  
692 T. Thordarson, S. Self, G. Larsen, S. Rowland, and A. Hoskuldsson, *Spec. Publ. IAVCEI*, 2,  
693 33–51.
- 694 Hon, K., J. Kauahikaua, R. Denlinger, R., and K. Mackay (1994), Emplacement and inflation of  
695 pahoehoe sheet flows: Observations and measurements of active lava flows on Kilauea  
696 Volcano, Hawaii. *Geol. Soc. Am. Bull.*, 106 (3), 351–370.
- 697 James, M. R., H. Pinkerton, and S. Robson (2007), Image-based measurement of flux variation  
698 in distal regions of lava flows, *Geochem. Geophys. Geosys.*, 8(3),  
699 doi:10.1029/2006GC001448.

700 James, M.R., H. Pinkerton, M. and Ripepe (2010), Imaging short period variations in lava flux,  
701 *Bull. Volcanol.*, 72, 671-676, doi: 10.007/s00445-010-0354-y.

702 Kauahikaua, J., K. V. Cashman, D. A. Clague, D. Champion, J. T. Hagstrum (2002)  
703 Emplacement of the most recent lava flows on Hualalai Volcano, Hawaii. *Bull. Volcanol.* 64,  
704 229-253, doi: 10.1007/s00445-001-0196-8.

705 Keszthelyi, L., S. Self, and T. Thordarson (1999), Application of recent studies on the  
706 emplacement of basaltic lava flows to the Deccan Traps. *Memoirs – Geological Society of*  
707 *India*, 43, 485–520.

708 Mazzarini, F., M. T. Pareschi, M. Favalli, I. Isola, S. Targuini, S., and E. Boschi (2005),  
709 Morphology of basaltic lava channels during the Mt. Etna September 2004 eruption from  
710 airborne laser altimeter data, *Geophys. Res. Lett.*, 32, L04305, doi: 10.1029/2004GL021815.

711 McGetchin, T., and J. Eichelberger (1975), Emplacement of the 1801 Hualalai lava flow,  
712 Hawaii, *Solid Earth Geosci. Res. Activ. LA-5956-PR*, Los Alamos Natl. Lab., Los Alamos  
713 NM.

714 Mei, C. C. (1966), Nonlinear gravity waves in a thin sheet of viscous fluid, *J. Math. Phys.*, 45,  
715 266–288.

716 Moore, H. J. (1987), Preliminary estimates of the rheological properties of 1984 Mauna Loa  
717 lava, in *Volcanism in Hawaii*, U.S. Geol. Surv. Prof. Pap., 1350, 1569–1588.

718 Nichols, R. L. (1939), Viscosity of lava, *J. Geol.*, 41, 270–302.

719 Oppenheimer, C. (1991) Lava flow cooling estimated from Landsat Thematic Mapper infrared  
720 data: the Lonquimay eruption (Chile, 1989) *J. Geophys. Res.* 96 (B13), 21,865-21,878.

721 Rose, S., and M. Ramsey (2009), The 2005 eruption of Kliuchevskoi volcano: Chronology and  
722 processes derived from ASTER spaceborne and field-based data, *J. Volcanol. Geotherm. Res.*,  
723 184, 367-380.

724 Rowland, S. K., and G. P. L. Walker (1990), Pahoehoe and aa in Hawaii: volumetric flow rate  
725 controls the lava structure, *Bull. Volcanol.*, 52, 615–628.

726 Shaw, H.R., and D.A. Swanson, (1970), Eruption and flow rates of flood basalts. In *Proceedings*  
727 *2<sup>nd</sup> Columbia River Basalt Symposium*, pp. 271-299, Eastern Washington State College Press,  
728 Cheney.

729 Wright, R., and L. P. Flynn (2003), On the retrieval of lava flow surface temperatures from  
730 infrared satellite data, *Geology*, 31, 893–896.

731 Wright, R., D. A. Rothery, S. Blake, and D. C. Pieri (2000), Improved remote sensing estimates  
732 of lava flow cooling: A case study of the 1991 to 1993 Mount Etna eruption, *J. Geophys. Res.*,  
733 105, 23,681-23,694.

734



735 Wright, R., H. Garbeil, and A. G. Davies (2010), Cooling rate of some active lavas determined  
736 using an orbital imaging spectrometer, *J. Geophys. Res.*, *115*, B06205, doi:10.1029/2009  
737 JB006536.

738

739

740 **Tables**

741 **Table 1.** Dissipation time constants  $\Gamma$  in seconds for eddy of radius  $R$  and viscosity  $\mu$ .

742

| Eddy radius,<br>$R$ (m) | Lava dynamic viscosity, $\mu$ (Pa s) |      |      |       |
|-------------------------|--------------------------------------|------|------|-------|
|                         | 10                                   | 100  | 1000 | 10000 |
| 0.5                     | 65                                   | 6.5  | 0.65 | 0.065 |
| 1                       | 260                                  | 26   | 2.6  | 0.26  |
| 2                       | 1040                                 | 104  | 10.4 | 1.04  |
| 5                       | 6500                                 | 650  | 65   | 6.5   |
| 10                      | 26000                                | 2600 | 260  | 26    |

743

744

745

**Table 2.** Parameters used to calculate lava core cooling

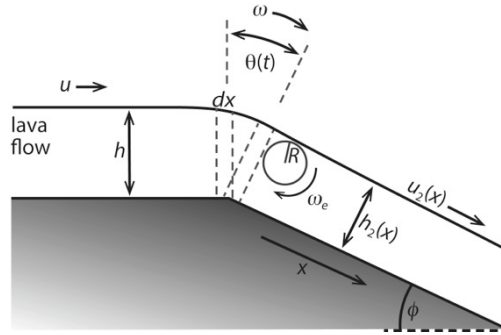
|                                |   |
|--------------------------------|---|
| Flow depth, $h$                | 5 m                                     |
| Initial temperature, $T_o$     | 1330 K                                  |
| Lava density, $\rho$           | 2600 kg m <sup>-3</sup>                 |
| Lava specific heat, $C_p$      | 1225 J kg <sup>-1</sup> K <sup>-1</sup> |
| Lava emissivity, $\varepsilon$ | 1                                       |
| Flow velocity, $u$             | 0.2 m s <sup>-1</sup>                   |

746

747 **Figures**

748

749

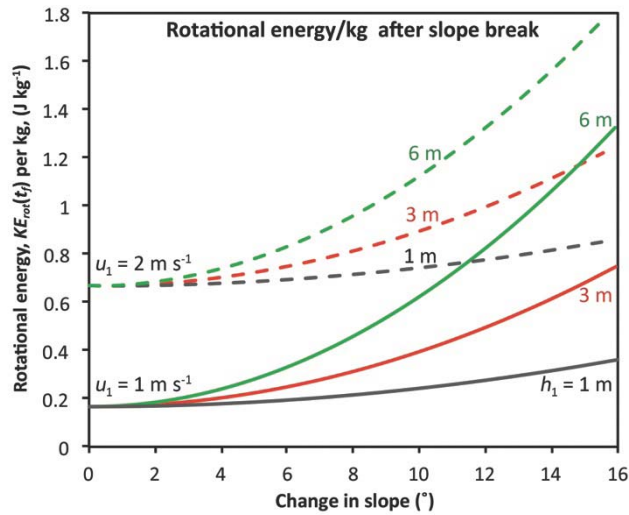


750

751 **Figure 1.** Geometry of a lava flow encountering a slope break. A lava column of height  $h$  and  
752 thickness  $dx$  (dashed lines) rotates through an angle  $\theta$  with angular velocity  $\omega$  as it pivots over  
753 the slope break, thereby imparting rotational energy to the flow and producing an eddy of radius  
754  $R$  and angular velocity  $\omega_e$ . On the new slope  $\phi$ , the flow takes on new velocity  $u_2$  and depth  $h_2$ .

755

756



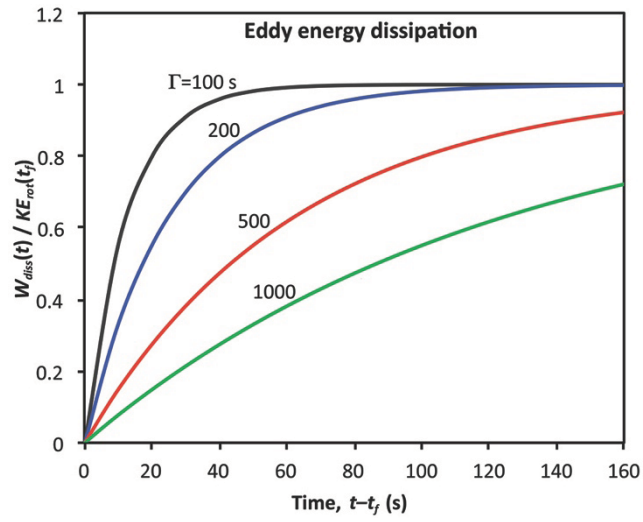
757

758

759 **Figure 2.** The absolute value of the exit rotational energy  $KE_{rot}(t_f)$  per kg as a function of the  
760 change in underlying slope at the slope break. The reference case is taken as  $u_1 = 1 \text{ m s}^{-1}$  and  $h_1$   
761  $= 1 \text{ m}$  for the incident flow. The rotational energy changes by a factor of 2 over slope changes up  
762 to  $15^\circ$  (solid gray curve). For flows of thickness 3 and 6 m, the rotational energy changes by  
763 factors of 4 and 7 (red and green curves), respectively, demonstrating the sensitivity of rotational  
764 energy to slope for thicker flows. For comparison, the dashed curves show the effect of a greater  
765 incident velocity ( $u_1 = 2 \text{ m s}^{-1}$ ): the dependence on slope is essentially the same as for the lower  
766 velocity, but there is an overall increase in the rotational energy.

767

768



769

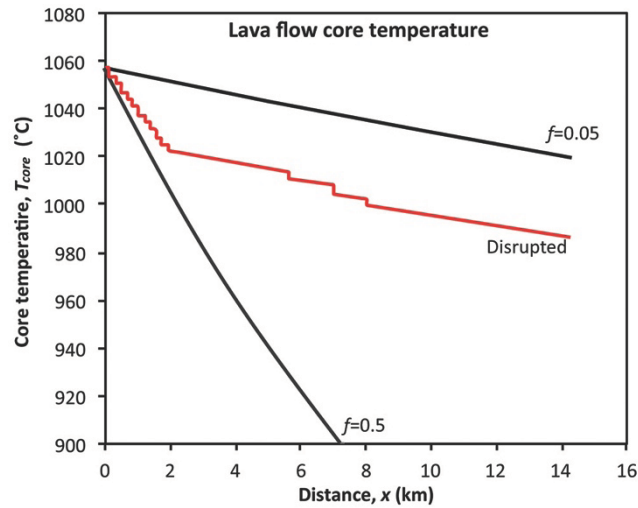
770 **Figure 3.** Eddy energy dissipation as a function of time for  $\Gamma = 100, 200, 500$  and  $1000$  s from

771 equation (16).

772

773

774



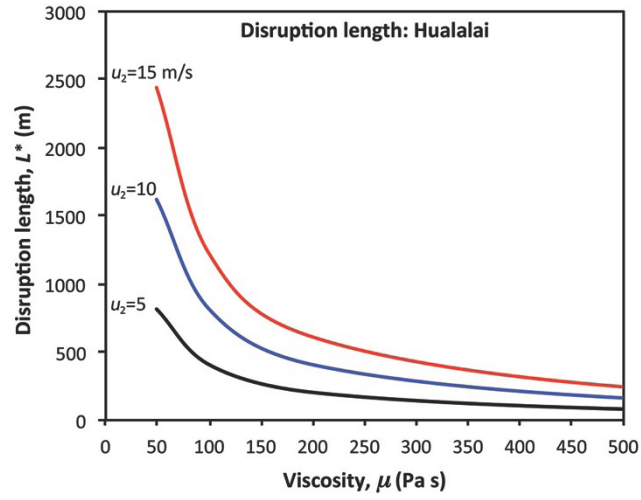
775

776 **Figure 4.** Theoretical temperature profiles along the length of a hypothetical flow for three  
777 different values of  $f$ . The dark curves assume constant core exposure fractions of  $f = 0.05$  and  $f =$   
778  $0.5$ . For comparison, the red curve shows the strong influence of the  $T^4$  radiation term when the  
779 flow surface is disrupted by eddies. Twelve 60 m segments of disruption with  $f = 0.9$  were  
780 inserted in the first 2 km of the flow, followed by three others further downstream.

781

782

783



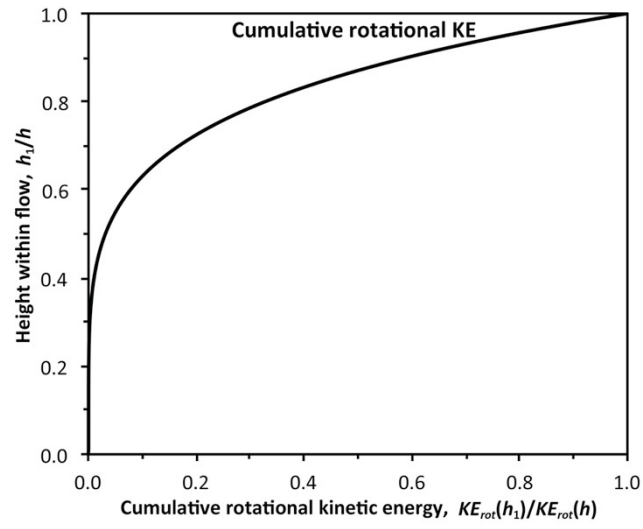
784

785 **Figure 5.** Disruption lengths as a function of viscosity for the lava flow from the 1801 Hualalai  
786 eruption for three plausible flow velocities. See text for discussion of parameters.

787

788

789



790

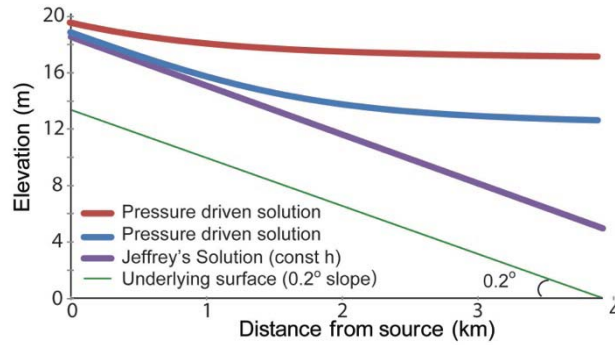
791 **Figure A1.** Cumulative rotational kinetic energy for a laminar flow pivoting over an abrupt slope

792 break as a function of the relative depth  $h_1$  within a flow of thickness  $h$ .

793



794



795

796

797 **Figure B1.** Comparison of steady-state gravity and pressure driven solutions with constant  
798 Jeffreys' solution  $h_J$  for the flow depth. For clarity of illustration, the slope is taken as  $0.2^\circ$ .  
799 Once the flow rate, slope and viscosity are fixed, small increases in the flow depth at the source  
800 cause a significant departure from the constant Jeffreys' flow depth. At 3–4 km from the source,  
801 the flow has more than doubled beyond  $h_J$ .

802

803

804

805

806

807